14th International Symposium on Turbulence and Shear Flow Phenomena (TSFP14)
Heidelberg, Germany, July 28–31, 2026

THE ROLE OF ANALYTICAL AND PART-ANALYTICAL APPROACHES IN PARTICLE-LADEN FLOWS

Rama Govindarajan
International Centre for Theoretical Sciences
Tata Institute of Fundamental Research
Bengaluru-560089, India
rama@icts.res.in

Anup Kumar
Nonlinear and Non-equilibrium Physics Unit
Okinawa Institute of Science and Technology
Okinawa 904-0495, Japan
anup.kumar@oist.jp

Saumav Kapoor
International Centre for Theoretical Sciences
Tata Institute of Fundamental Research
Bengaluru-560089, India
saumav.kapoor@icts.res.in

ABSTRACT

Particle-laden flows are usually extremely complex and practically impossible to solve computationally. If they could be broken up into building blocks which could be approached by simpler solution methods, that would help elucidate the physics as well as provide handles for machine learning algorithms. This paper discusses two such simplifications, in the form of particles near one or two vortices, as a building block of particle-laden turbulence, and the stability analysis of a model shear flow where gradients in particle concentration drive instability. Mathematical and other details are given here, whereas the talk will focus on physical aspects.

BACKGROUND

This paper is designed to accompany the talk in the Symposium on this topic. The main references on which it is based are Ravichandran & Govindarajan (2015); Ravichandran *et al.* (2014); Kapoor *et al.* (2024); Kumar & Govindarajan (2024); Joshi *et al.* (2025); Rajarshi & Govindarajan (2026). While the talk will focus on the physics, we focus here on the mathematical background. The talk will discuss further studies as well.

Particle-laden and droplet-laden flows are common in geophysical contexts and in industrial processes. By their very nature they present a problem of enormous complexity. Among the least understood aspects is why clustering or declustering of particles occurs. Even if we start with a homogeneous particulate distribution, the distribution rarely remains homogenous as the dynamics proceeds. In fact extremely large levels of clustering can take place, often aided by turbulence, or by instability. And it is very important to understand this, for existential and practical reasons. Clustering results in enhanced possibility for inter-particle collisions, which are critical for various natural phenomena including raindrop formation (Falkovich *et al.*, 2002; Wilkinson *et al.*, 2006), reproduction among small organisms (Guasto *et al.*, 2012) and planet formation (tan, 1996; Bracco *et al.*, 1999). Isn't it mind-boggling to imagine that we are all here because long ago, dust particles around our Sun somehow defied 'normal' logic to come together to form Earth. And we survive because tiny droplets in a cloud defy the same logic all the time to provide us with rain. Below we shall discuss one case of vorticity-enhanced clustering, while making references to raindrop formation in clouds, and one of a special instability that only particle-laden flows can display, using particle-laden channel flow as an example.

Why this problem is hard

A cloud, especially a stratocumulus, is often in rather violent turbulent flow. Its horizontal extent could be in tens (or even hundreds) of kilometres, and its vertical extent over 10 kilometres. Every cubic centimetre of this cloud could contain $O(10^3)$ tiny droplets of about 10 micron size. If we were to solve exactly for just one single cubic metre of this flow, it is easy to realise that imposing no-slip and no-penetration boundary conditions on the 10^9 droplets within it, and solving for the dynamics of each of them, is impossible. Now let us imagine a river carrying sediment particles, also in turbulent motion. At their mouth rivers can have a high particle loading. So the same argument holds, and exact simulations at these large scales are impossible. Still, particle-resolved simulations (Izbassarov *et al.*, 2018; Vow, 2014) are making great progress, and small-scale physics can be gleaned from them. On the other hand there have been a large number of direct numerical simulations of turbulent flows (Squires & Eaton, 1991; Marshall, 2005; Bec *et al.*, 2007) which typically are at higher Reynolds number that the particle-resolved simulations, but where particle motion is approximated in different ways. These studies must go hand-in-hand with modelling. Hierarchies of modelling and approximate methods have been traditionally adopted, and these have become more sophisticated over the decades. Ultimately, such problems might need to be solved by physics-informed machine learning tools, but there is much to be learned, even today, by analytical methods which include paper and pen studies.

Reduction into tractable questions

In our definition of analytical studies we include all those where pen and paper play a part. We reduce the description of the problem to ordinary-differential-equations which are then solved numerically. Two such methods are discussed here. (i) Turbulence is given a minimal description and (ii) the instability of the laminar flow is studied.

In the first problem, we define and study a building block of particulate or droplet turbulence: inertial stokesian particles in the vicinity of vortices. Vortices are known to be the sinews of turbulence (Moffatt *et al.*, 1994). Much of turbulence can be explained by the dynamics of coherent vortices within it. Small inertial particles are known to centrifuge out of vortical regions and cluster into regions of strain. How this affects collisions is not completely solved as yet (Falkovich *et al.*, 2002; Wilkinson *et al.*, 2006; Ravichandran & Govindarajan, 2022).

We begin with small inertial spherical particles in the vicinity of a single vortex. We will discuss a singular perturbation problem that presents itself here, and relate it to the formation of caustics. Following this, we move on to a co-rotating vortex pair. This problem is addressed numerically, although with an analytically prescribed mean flow. Here we will see how clustering into manifolds of smaller than the spatial dimension happens.

In the second problem we set up the stability analysis of a channel flow where particle loading is inhomogeneous. We will show how the gradient in particle concentration affects the critical-layer balance and leads to a new instability, which we term the 'Overlap' instability.

SMALL INERTIAL PARTICLES NEAR A POINT VORTEX

It is instructive to begin with the simplest building block: of a small spherical particle in one-way coupling near a single point vortex. This seemingly trivial, effectively one-dimensional, problem has an amazing boundary-layer structure which leads to caustics in a special region, and allows for selective particle agglomeration (Ravichandran & Govindarajan, 2022, 2015; Deepu *et al.*, 2017). The flow field is given by the velocity $\mathbf{u}_d = u_\theta = \Gamma/r\ \hat{\theta}$, where (r,θ) are cylindrical polar coordinates, where $\pi\Gamma$ is the circulation of the vortex. The particle velocity $\mathbf{v}$ satisfies the Gatignol-Maxey-Riley equation (Gatignol, 1983; Maxey & Riley, 1983), which in its simplest form reads

$$\frac{d\mathbf{v}_d}{dt} = -\frac{1}{\tau}\left[\mathbf{v}_d - \mathbf{u}_d\right]. \tag{1}$$

The subscript d stands for a dimensional quantity, and τ is the particle response time. Choosing τ and $L \equiv (\Gamma\tau)^{1/2}$ as time and length scales respectively, and rewriting in cylindrical polar coordinates, we have, for the radial coordinate r of the particle

$$\ddot{r} + \dot{r} = \frac{\zeta^2}{r^3}, \quad \dot{\zeta} + \zeta = 1, \tag{2}$$

where $\zeta = r^2\dot{\theta}$ is the nondimensional angular momentum of the particle. The solution is a monotonic centrifugation out of the vortex vicinity while executing spiral motion. This is a parameter-free equation valid for a particle of any response time, for a vortex of any strength, so long as the particle Reynolds number $Re_p \equiv a(v-u)/\nu$ is small. Here a is the particle radius and ν the kinematic viscosity of the fluid. The nondimensionalisation chosen obscures the fact that this is a singular perturbation problem, but simple rescaling will make this evident. At extremely short times and small r the acceleration of the particle becomes important, whereas at late times, or when $r > O(1)$, it is unimportant, and the particle executes a Fermat spiral (Ravichandran & Govindarajan, 2022), satisying

$$r^3\dot{r} = 1.$$

Particle collisions can only occur at short times and small r, and in particular, within a caustics radius of $0.55L$. If we repeat this exercise with a polydisperse set of particles, the caustics radius goes up steeply with polydispersity. This speaks to the power of polydispersity. And in turbulence, powerful small scale vortices are usually of gaussian (Lamb-Oseen) vortex profiles (Ramadugu *et al.*, 2022), for which the point vortex approximation is a good one. We thus have a solve-for-one and get-all-the-answers situation which lends itself to rapid solutions by machine learning, a worthy replacement for computing a billion particle trajectories in an elaborate fashion. In cloud turbulence only a very small minority of vortices are such that L will be outside the vortex radius, such that caustics can occur. But such a small fraction is sufficient to trigger droplet growth if the cloud Reynolds number is above a million, as obtained in the order of magnitude estimate of Ravichandran & Govindarajan (2022). Though understanding inertial particle dynamics in turbulent flows is partially served by studying the motion of particles in model vortical flows (Tio *et al.*, 1993; Lasheras & Tio, 1994; Marcu *et al.*, 1995; Raju & Meiburg, 1997; Marshall, 1998; Varaksin & Ryzhkov, 2022), turbulence of course consists of more than vortices, so this will provide only incomplete answers. But many aspects of turbulence can be approximated for this context by a small set of canonical toy problems.

Spherical particles near a co-rotating vortex pair

We have seen how particles behave in the vicinity of a single vortex. Turbulence consists of a myriad range of vortices and particles may respond to combinations of them. In this section which heavily follows Kapoor *et al.* (2024), we show how extreme clustering can occur in the neighborhood of just a pair of identical vortices. Moreover we will see how particles get trapped within closed streamlines.

Sapsis & Haller (2010), making the small Stokes number and field equation approximation, showed that

$$\nabla\cdot\boldsymbol{v} = St\left\{|\boldsymbol{\omega}(\boldsymbol{x},t)|^2 - |\boldsymbol{S}(\boldsymbol{x},t)|^2\right\} = StQ\,, \tag{3}$$

where Q is the Okubo-Weiss parameter, and $\boldsymbol{\omega}$ and $\boldsymbol{S}$ are the antisymmetric and symmetric parts of the velocity gradient tensor respectively. This finding indicates that particles must evacuate regions of closed streamlines. But in a frame of reference rotating at the angular speed Ω, this is modified (Ravichandran *et al.*, 2014) to

$$\nabla\cdot\boldsymbol{v} = -St\left\{|\boldsymbol{S}(\boldsymbol{x},t)|^2 - |\boldsymbol{\omega}(\boldsymbol{x},t)|^2 + 2\Omega^2\right\} = StQ_{rot}\,, \tag{4}$$

allowing particles of small St to be trapped within closed streamlines *in the rotating frame*.

A pair of Lamb-Oseen vortices of identical strength, Γ, is a simple system which allows for such a region. We assume no gravity and an inviscid evolution of the vortices for simplicity, and choose the ratio of vortex core width b to inter-vortex separation d to be small, $b/d \ll 1$. Then the vortices simply revolve around each other on a circle of constant diamater d with an angular speed $\Omega = \Gamma/\pi d^2$, in accordance to the Biot-Savart law, as schematically shown in fig. 5(a). We use d and the co-rotation time period $T = 2\pi/\Omega$ to non-dimensionalise the system. The flow field is completely solvable and steady in the rotating frame. The separatrices and some streamlines in the co-rotating frame are shown in fig. 5(a), and the region of interest with closed streamlines, where particles cluster, is highlighted in blue (region II).

In this flow field, consider a dilute suspension of (one-way coupled) particles, each modelled as a rigid sphere with a small radius a, with a finite particle-to-fluid density ratio $\beta = \rho_p/\rho_f$. The dynamics of such particles is governed by the Gatignol-Maxey-Riley equations, written this time in their complete non-dimensional form (Gatignol, 1983; Maxey & Riley, 1983) as

$$\frac{d\hat{\boldsymbol{r}}}{dt} = \hat{\boldsymbol{v}}\,, \tag{5a}$$

$$\begin{aligned}\frac{d\hat{\boldsymbol{v}}}{dt} = &-\frac{(\hat{\boldsymbol{v}} - \hat{\boldsymbol{u}}(\hat{\boldsymbol{r}}))}{St} + R\frac{D\hat{\boldsymbol{u}}}{Dt}(\hat{\boldsymbol{r}}) \\ &- \sqrt{\frac{3R}{\pi St}}\left[\frac{(\hat{\boldsymbol{v}}_0 - \hat{\boldsymbol{u}}_0)}{\sqrt{t}} + \int_0^t ds \frac{1}{\sqrt{t-s}}\left\{\frac{d}{ds}(\hat{\boldsymbol{v}}(s) - \hat{\boldsymbol{u}}(\hat{\boldsymbol{r}}(s)))\right\}\right],\end{aligned} \tag{5b}$$

where the subscript 0 stands for a quantity at the initial time, $R = 3/(2\beta+1)$ is the density factor and the Stokes number $St = \tau_p/T$ measures the relative particle response time. The forcing terms on the right-hand side of eq. (5b) are the viscous Stokes drag, the force due to local fluid acceleration (which includes the added mass and pressure drag effects), and the Basset-Boussinesq History (BBH) force respectively. The values of $R = 0, 1, 3$ correspond to infinitely dense, neutrally buoyant and light particle (like a bubble) respectively. Clustering of particles in the vortex vicinity is non-trivial when the particle is denser than the fluid, making $0 < R < 1$ as the regime of interest. Further, the above equation assumes that each of particle Reynolds number, $Re_p = a|\boldsymbol{v}_d(t) - \boldsymbol{u}_d(\boldsymbol{r}_d, t)|/\nu$, shear Reynolds number, $Re_s = a^2|\nabla \boldsymbol{u}_d|/\nu$, as well that Faxén corrections are negligible; these are valid assumptions for sufficiently small particles. The dynamics of such a suspension is better understood in the co-rotating frame in which the background flow is steady. In this frame the equations of motion transform to

$$\frac{d\boldsymbol{r}}{dt} = \boldsymbol{v}, \tag{6a}$$

$$\begin{aligned}\frac{d\boldsymbol{v}}{dt} = &-\frac{\boldsymbol{v}_{rel}}{St} + R\left\{\frac{D\boldsymbol{u}}{Dt}(\boldsymbol{r}) + 4\pi\boldsymbol{e}_z \times \boldsymbol{u}(\boldsymbol{r}) - 4\pi^2\boldsymbol{r}\right\} \\ &- \sqrt{\frac{3R}{\pi St}}\left\{\frac{\boldsymbol{v}_{rel,0}}{\sqrt{t}} + \int_0^t ds\, \frac{d\boldsymbol{v}_{rel}(s)/ds + (2\pi\boldsymbol{e}_z) \times \boldsymbol{v}_{rel}(s)}{\sqrt{t-s}}\right\} \\ &- 4\pi\boldsymbol{e}_z \times \boldsymbol{v} + 4\pi^2\boldsymbol{r},\end{aligned} \tag{6b}$$

where $\boldsymbol{v}_{rel} \equiv \boldsymbol{v} - \boldsymbol{u}(\boldsymbol{r})$ is the particle slip velocity, and all the variables are measured in the co-rotating frame. Right now we focus on the case when BBH force is ignored, but comparisons with the BBH force were done in (Kapoor *et al.*, 2024).

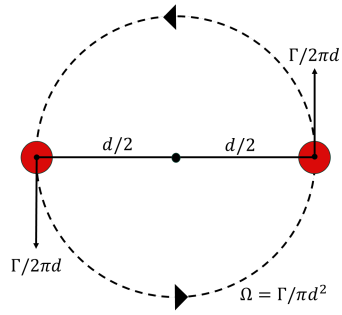

(a)

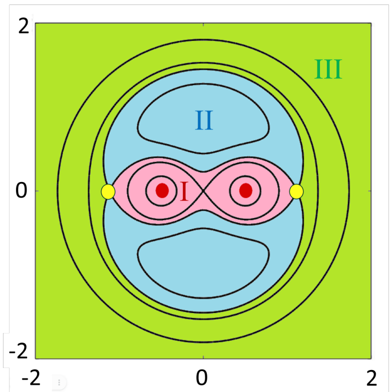

(b)

Figure 1: (a) Schematic showing the identical vortex pair executing circular motion at a constant rate. (b) Vortex locations (red dots) are $(\pm 1/2, 0)$ and some representative tracer-particle trajectories (closed orbits shown in black lines), including the separatrices, are shown in the rotating frame of reference. Inertial particle attractors are primarily found in region II (shaded blue). Regions I (shaded pink), II and III (shaded green) are separated by heteroclinic orbits emanating from the hyperbolic fixed points, shown in in yellow.
Region III contains simple closed orbits encircling both vortices.

However, the case without BBH qualitatively describes the diversity in dynamics.

The spatial regions relevant for the particle dynamics in the current problem are highlighted in fig. 5(b). Region I (shaded red) behaves akin to a single vortex vicinity, where particles display (the already discussed) centrifugation radially outward from the vortices. Trapping only occurs in region II (shaded blue), which contains closed streamlines. Going further from the origin and into the far-field region III (shaded green), particles increasingly perceive the vortex pair as a single vortex of twice the strength, and simply centrifuge radially outward and, as a result, escape.

Within region II particles can be attracted towards fixed points, limit cycles or chaotic (strange) attractors co-rotating with the vortices, or not be trapped at all, depending on R and St. The number of particles that get trapped can be quantified by the basin of attraction (BoA), the size and shape of which also varies with R and St. For $R = 0.84$ ($\beta = 1.285$), these three variety of attractors and their corresponding BoA (with $\boldsymbol{v}_{initial} = 0$) is shown in in fig. 2. In fact, near neutrally buoyant particles display a period-doubling route to chaos, followed by a crisis beyond which all particles escape, with in-

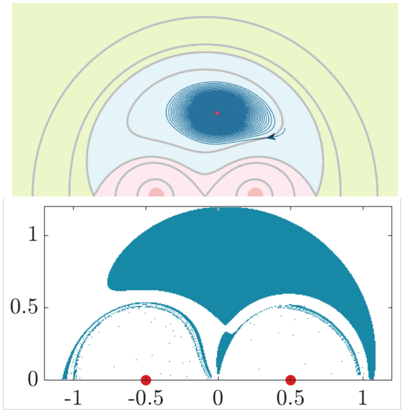

(a) $St = 0.09$

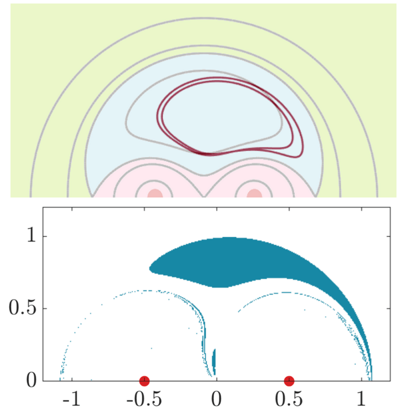

(b) $St = 0.22$

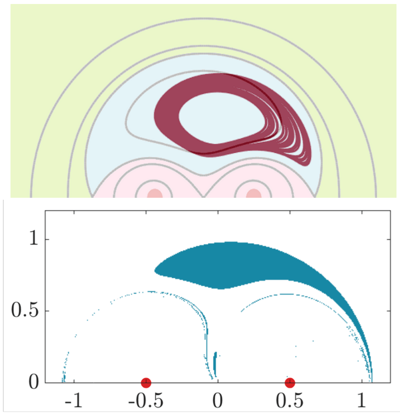

(c) $St = 0.24$

Figure 2: Typical attractors shown in maroon (top) and their corresponding basins of attraction (bottom) for a finitely-dense inertial particle with the desnity parameter $R = 0.84\,(\rho_p/\rho_f \approx 1.3)$ and increasing Stokes number St, without the BBH force. Vortex centres, in the rotating frame, are shown as red dots. In (a) the particle spirals (shown in blue) into a fixed point attractor, while in (b) the particle is trapped into a limit cycle of period 2 and in (c) in a strange (chaotic) attractor respectively. The orbits are overlaid on the the background flow with highlighted regions for clarity of their scale and location. In the lower half-plane, dynamics are symmetric with a 180° rotation about the out-of-plane axis through the origin.

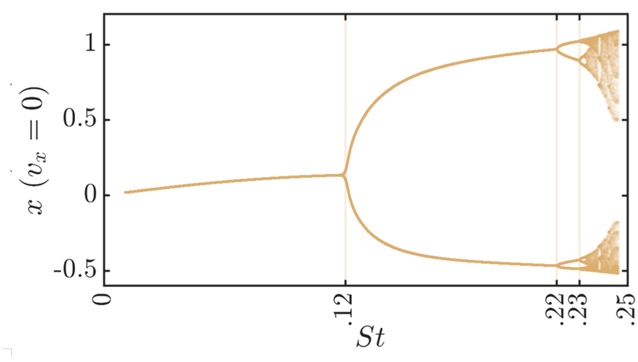

Figure 3: Bifurcation diagram for $R = 0.84\ (\rho_p/\rho_f = 1.285)$ without the BBH force. The attractor is a fixed point below $St = 0.12$, while for $0.12 < St < 0.22$ it is a period-1 limit cycle, followed by period doubling route to chaos as the Stokes number increases. There are no asymptotic attractors beyond $St_{crit} = 0.24675$ where a crisis occurs.

creasing St and fixed R. This is shown for $R = 0.84$ in fig. 3 where the ordinate extrema of the asymptotic states are plotted with increasing St to construct a bifurcation diagram. The St gap between consecutive bifurcations was checked to go down asymptotically as the Fiegenbaum number, with chaos setting in at $St = 0.232$. Then there is sharp cut-off (crisis) at a critical $St_{crit} \approx 0.25$, beyond which BoA drops to zero suddenly and no trapping occurs for any initially finite volume of particles.

Trapping in these attractors signifies that particles eventually occupy spatial regions with fractal dimension of less than 2 (which have zero volume), despite starting out in a spatial region of fractal dimension 2 (having non-zero volume). This focussing of particles is a signature of caustics formation and causes extreme clustering.

Moving on to higher density ratios, we show bifurcation diagrams for $R = 0.5,\ 0.48,\ 0.2$. Here the variation in the nature of attractors with St becomes even more non-trivial. One can have intermittent windows of St where no particle trapping occurs, as shown in fig. 4(b,c). Not only that, period doubling (even till chaos) can be followed by (the rarer) period halving back to fixed point, as shown in fig. 4(a,b). This shows that the complexity of attractors as well as the propensity of trapping can vary non-monotonically with St, in contrast to monotonic trends in St that the community tends to expect.

STABILITY OF PARTICLE-LADEN CHANNEL FLOW

0.1 The basic idea

We study the stability of a channel flow with non-uniform particle loading (Kumar & Govindarajan, 2024), as shown in Fig.5. We believe this study can provide intuition for a host of sediment and other particle-laden shear flows. In the case of the flow of a clean fluid, we know that Tollmien-Schlichting (TS) modes cause the first linear instability, at a Reynolds number $R = 5772.2$, where $R \equiv HU/\nu$, H, U and ν respectively being the channel half-width, centreline velocity and the fluid kinematic viscosity. Viscous instability is always interesting because we normally expect viscosity to work against instability and to smooth things out. But a clean channel is inviscidly stable, and viscously unstable. The reason again is singular perturbation (Lin, 1945*b*). The reader is requested to

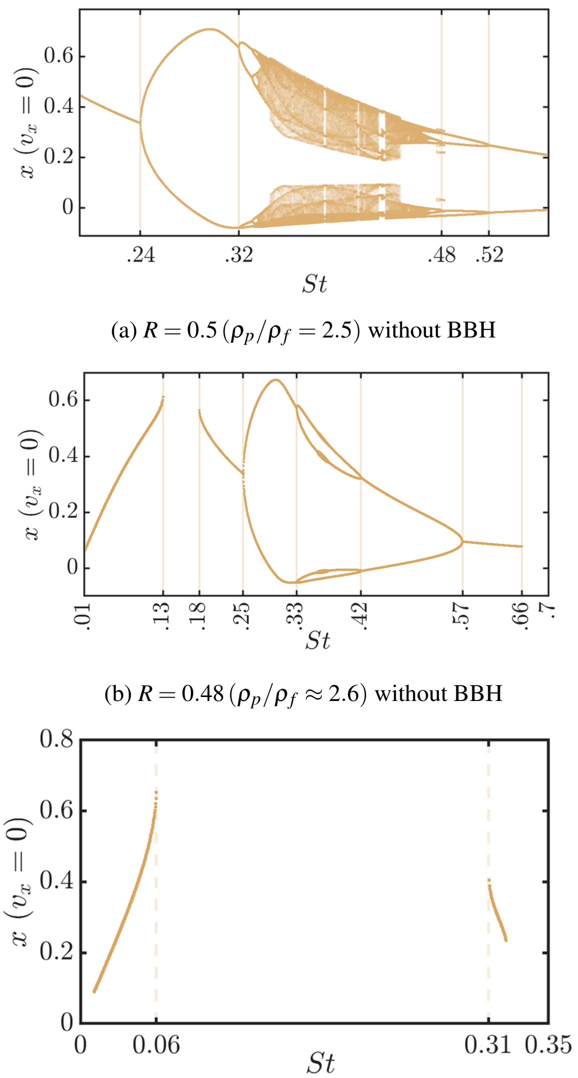

(a) $R = 0.5\,(\rho_p/\rho_f = 2.5)$ without BBH

(b) $R = 0.48\,(\rho_p/\rho_f \approx 2.6)$ without BBH

(c) $R = 0.2\,(\rho_p/\rho_f = 7)$ without BBH

Figure 4: Bifurcation diagrams for different representative density ratios. In (a), (b) and (c) the BBH force is neglected. On the ordinate are the extrema of the x-coordinate of the asymptotic trajectories.

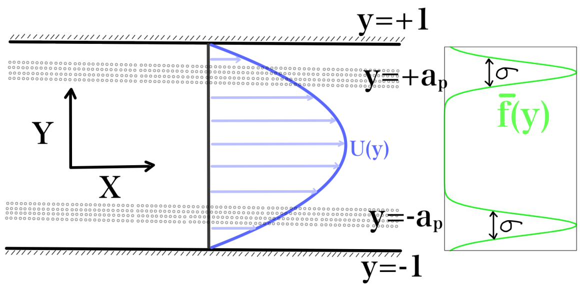

Figure 5: Schematic of channel flow with non-uniform particle loading. The velocity profile is parabolic, and the base particle profile $\bar{f}(y)$ shown in green is a pair of gaussians of width σ centred around $y = \pm a_p$.

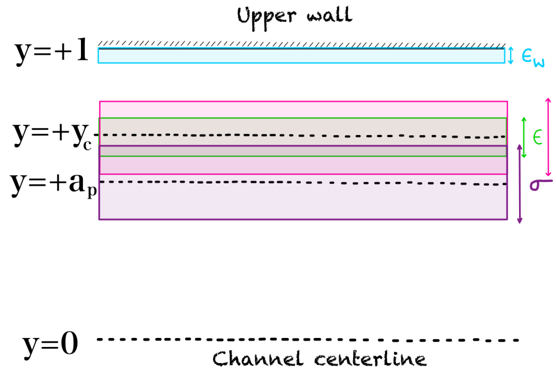

Figure 6: Schematic showing layers of rapid variations in flow quantities, and defining the wall-normal variable y. The wall layer WL shown in blue represents the location of peak dissipation. Shown in green and pink are the critical layers CLs where disturbance kinetic energy production is large, for the fluid and particles, respectively. Shown here is a condition of overlap of the particle layer (in purple) with the CL. We show the top half of the channel; the other half being symmetric.

refer to Kumar & Govindarajan (2024) for details, but here we give the basic outline of how particle-laden layers enter this singular perturbation. In the clean laminar flow through a channel, there are two layers of importance: the critical layer, CL and the wall layer, WL, where all the action happens. CL is primarily where disturbance kinetic energy is produced. It is then transported to other parts of the channel including WL, where primarily it is dissipated. Whenever the net production exceeds the dissipation we get exponentially growing instability. For a clean channel this never happens when $Re < 5772.2$, where Re is the channel Reynolds number based on centerline velocity and channel half-width. But now, when particles occupy the CL, the fundamental balance gets disrupted, and we can get new modes of instability, at rather low Reynolds number, as seen in the example of Fig. 6. and moreover there is a non-zero gradient of mean particle concentration in this layer, magic happens, as we can see in figure 7. Two new modes of instability, caused by the existence of particles in the flow, are now seen. Why this happens is explained in the following subsection.

0.2 Perturbation energy production in the critical layer

When there are no particles, CL (of thickness $\varepsilon \sim Re^{-1/3}$ and where $U \sim c$) and WL (of thickness $\varepsilon_w \sim Re^{-1/2}$) were shown by Lin a long time ago to be layers where (Lin, 1945*b*,*a*, 1946) where viscous effects are important and gradients are large.

The linear stability problem may be posed as an eigenvalue problem for a given perturbation wavelength α where the eigenfunctions correspond to the nontrivial disturbance fields permissible, and the real and imaginary parts of the eigenvalue c yield the phase speed and growth rate of the perturbation respectively, with exponential growth of perturbations occurring for $c_i > 0$. In the stability operator of high Reynolds number shear flow (Drazin & Reid, 2004) for a clean fluid, it is usually seen that the highest derivative term in y is scaled by the inverse of the Reynolds number. Now even if the Reynolds

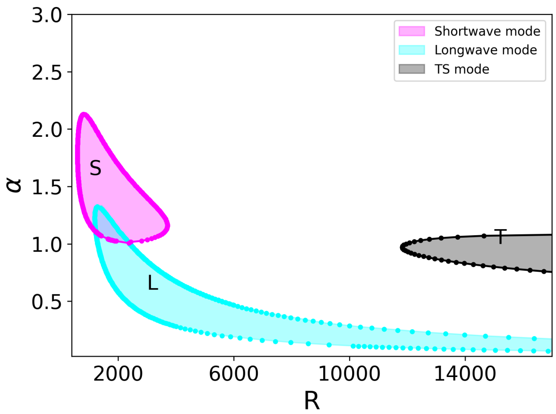

Figure 7: Three distinct modes of instability: S, L and T (shortwave, longwave and Tollmien-Schlichting respectively), shown by the shaded regions in the Reynolds-number (Re) wavenumber (α) plane. Here $f_{max} = 0.70$, $a_p = 0.75$, $\sigma = 0.1$ (see Fig. 5) and the particle Stokes number $St = 8 \times 10^{-4}$.

number approaches infinity, this term may not be dropped, because if it is, we will not be able to satisfy all the boundary conditions associated with the stability equation. This is thus a classical singular perturbation problem (Van Dyke, 1964), where the highest derivative term becomes as big as the terms on the left-hand side in some portions of the flow. We limit ourselves to the regime where $ReSt \sim O(1)$, which is reasonable for dilute particle suspensions at high Reynolds number. There are three layers we pay attention to on each side of the centreline, and these are shown in Fig. (6) for one half of the channel. A wall layer is also present, which has been discussed in Kumar & Govindarajan (2024). There are two critical layers: for the fluid and for the particle flow, of thickness ε and δ respectively (which will be shown below to be equal), and a layer where the particles are concentrated, of thickness σ. The basic idea is to show that when the particle-laden layer overlaps with the CLs, we have a dramatic effect on stability: two new modes of instability at Reynolds number an order of magnitude lower than the tradition Tollmien-Schlichting mode now occur, which are termed the S and L modes, for shortwave and longwave respectively. Conversely, when the particle layer and the CLs are well-separated, we refer to this as the non-overlap condition, where the instability behaviour is very similar to what we would see in a clean channel. We therefore call the new instability modes “Overlap” modes. The scales $\varepsilon \ll 1$ and $\delta \ll 1$ are determined by standard singular perturbation techniques.

As shown in Kumar & Govindarajan (2024), Squire’s theorem can be extended to dusty channel flows with inhomogeneous loading, including variations in viscosity. Therefore, to obtain critical Reynolds numbers Re_{cr}, it is sufficient to consider the two-dimensional perturbations. The governing stability equations are:

$$\left[(U_* - c)(D^2 - \alpha^2) - U_*''\right]\psi + D(J\bar{f}'\psi) = \frac{1}{i\alpha Re}\left[\bar{\mu}(D^2-\alpha^2)^2 + 2\bar{\mu}'D^3 + \bar{\mu}''D^2 - 2\alpha^2\bar{\mu}'D + \alpha^2\bar{\mu}''\right]\psi + \frac{1}{Re}\left[U'D^2 + 2U''D + U''' + \alpha^2 U'\right]\mu, \quad \text{and} \tag{7}$$

$$-(U-c)\gamma\mu + \left[-i\alpha RS\mathscr{M}^2U'\bar{f}' + (\mathscr{M}\bar{f})'\right]\psi = 0, \tag{8}$$

where

$$U_* \equiv U + J\bar{f}, \quad \mathscr{M} = \frac{1}{1 + i\alpha(U-c)StRe}, \quad J = (U-c)\mathscr{M}, \tag{9}$$

$$u_y = -i\alpha\psi \tag{10a}$$
$$u_x = D\psi \tag{10b}$$
$$v_x = \mathscr{M}u_x - (\mathscr{M}^2 StReU')u_y \tag{10c}$$
$$v_y = \mathscr{M}u_y \tag{10d}$$

The operator $D \equiv d/dy$, and a prime denotes a derivative in y of a mean quantity. The boundary conditions are:

$$\psi(y=\pm1) = D\psi(y=\pm1) = \mu(y=\pm1) = 0 \tag{11}$$

For given mean flow $U(y)$ streamwise wavenumber α, base particle loading $\bar{f}(y)$, particle to fluid density ratio, and fixed Re and St, equations 7 to 11 define an eigenvalue problem, which yields a spectrum of eigenvalues c and corresponding eigenfunctions, $(\psi(y), \mu(y))$. If even one eigenvalue has a positive imaginary part, i.e., $c_{im} > 0$, we have an exponential growing mode.

In the limit of $\gamma \to \infty$, we have $\bar{\mu} = 1$ and $\mu = 0$, so equation (7) becomes

$$\left[(U_* - c)(D^2-\alpha^2) - U_*''\right]\psi + (J\bar{f}')'\psi + (J\bar{f}')D\psi = \frac{1}{i\alpha R}(D^2-\alpha^2)^2\psi \tag{12}$$

and is now decoupled from equation (8). When there is no particulate suspension, we have $\bar{f} = 0$, and the system (12) reduces to the well-known Orr-Sommerfeld equation.

In the following part of this section we carry out some algebra, only to show how the basic balance in the CL is affected by overlap conditions. We do not solve the resulting CL equations. We derive equations within the critical (inner) layer in the inner variables ξ and λ, defined as

$$\xi = \frac{y - y_c}{\varepsilon}, \quad \text{and} \quad \lambda = \frac{y - y_c}{\delta} \tag{13}$$

and will select ε and δ to ensure that the derivatives of the fluid velocity components in ξ and the particle velocity components in λ are $O(1)$. In addition, we find it useful to define

$$\chi = \frac{y - a_p}{\sigma}. \tag{14}$$

We now write the relevant variables in the form of series expansions within the critical layer as

$$u_y = \sum_{n=0}^{\infty}\varepsilon^n u_{y,n}(\xi), \quad v_y = \sum_{n=0}^{\infty}\delta^n v_{y,n}(\lambda), \quad \text{and} \quad v_x = \sum_{n=0}^{\infty}\delta^n v_{x,n}(\lambda). \tag{15}$$

In this layer the mean flow may be written as

$$U(y) - c = (y - y_c)U_c' + \frac{(y - y_c)^2}{2} U_c'' + \cdots. \qquad (16)$$

The continuity equation can be used to further simplify the expressions. We have

$$\sum_{n=0}^{\infty} \varepsilon^n \left[i\alpha u_{x,n} + \frac{1}{\varepsilon} D_\chi u_{y,n} \right] = 0. \qquad (17)$$

Constructing hierarchies of equations of different powers of ε yields

$$u_{y,0} = 0 \qquad (18)$$

and shows that the coefficient of a particular power of ε in u_x is related to one which is an order higher in u_y. This is a natural consequence of incompressibility. For the particle field, from equations (10), (15) and (16), we get

$$\left[U - c - \frac{i}{\alpha StRe} \right] v_x = i\frac{U'}{\alpha} v_y + \frac{1}{\alpha^2 StRe} Du_y. \qquad (19)$$

At the next two orders, using equation (19) as well as the incompressibility condition $D_\xi u_{y,1} = -i\alpha u_{x,0}$ in the critical layer,

$$v_{x,0} = u_{x,0}, \qquad (20)$$

$$v_{x,1} = \frac{\varepsilon}{\delta} \left\{ \frac{i}{\alpha} D_\xi u_{y,2} - i\alpha StReU_c'\xi v_{x,0} \right\} - StReU_c' v_{y,1}. \qquad (21)$$

This yields $\delta \sim \varepsilon$, and without loss of generality, we choose $\delta = \varepsilon$. The critical layer thickness as perceived by the fluid and the particles is thus identical.

Using the third row of the matrix equation (12) along with equations (15) and (16), and collecting terms at the lowest order in the expansion, we obtain

$$v_{y,0} = u_{y,0}, \qquad (22)$$

which we know to be 0 from equation (18). In other words, the expansions for the normal velocity components for the particles too begin one order higher than the streamwise component. At the next two orders, from the equation (10)

$$\left[U - c - \frac{i}{\alpha StRe} \right] v_y = -\frac{i}{\alpha StRe} u_y \qquad (23)$$

we get

$$v_{y,1} = u_{y,1}, \quad \text{and} \quad v_{y,2} = u_{y,2} - i\alpha StReU_c'\xi v_{y,1}. \qquad (24)$$

From equations (15), (21), and (24), we can see that the components of $\mathbf{v}$ and $\mathbf{u}$ differ from each other only at order ε relative to their largest value in the critical layer. This is consistent with the expectation that the particle velocity field must closely follow the fluid velocity field for low Stokes numbers. This analysis yields a measure of the difference between the two.

We now consider only the overlap case, and under the limit $\varepsilon \sim \sigma$. Here $\varepsilon \sim (\alpha Re)^{-1/3}$, and $\frac{\varepsilon}{\sigma} \equiv \kappa$. , we obtain the dominant balance for fluid velocity in the CL from equation (10), (15) and (16), and the Taylor expansion

$$\bar{f} = \bar{f}_c + (y - y_c)\bar{f}_c' + \frac{(y - y_c)^2}{2} \bar{f}_c'' + \cdots, \qquad (25)$$

and we may rewrite this in terms of χ. The dominant balance in the CL now becomes

$$\left[U_c'(1 + \bar{f})\xi D_\xi^2 + iD_\xi^4 - \kappa(D_\chi \bar{f})U_c'(I - \xi D_\xi) \right] u_{y,1} = 0, \qquad (26)$$

and completely describes the CL. The variation of the particle concentration within the CL, estimated by $D_\chi \bar{f}$ is an important player in the CL balance, altering it fundamentally. We have thus established that the concentration profile will alter the fundamental nature of shear flow instability, only under overlap conditions. This effect would be absent with uniform particle loading, where we will have a factor $(1 + \bar{f})$ which merely rescales the Reynolds number.

CONCLUSIONS

We have considered two distinct problems in particle-laden flow and shown how analytical approaches can reveal some basic physics despite the complexity of the problem. In the lecture, we will also describe the instability of particulate arrays.

Acknowledgements

We acknowledge support from the Department of Atomic Energy, Government of India, under Project No. RTI4019. Rama Govindarajan thanks the ANRF JC Bose Grant for support.

REFERENCES

1996 Forming planetesimals in vortices. *Icarus* **121**, 158–170.

2014 Fluid–particle interaction in turbulent open channel flow with fully-resolved mobile beds. *Advances in Water Resources* **72**, 32–44.

Bec, J., Biferale, L., Cencini, M., Lanotte, A., Musacchio, S. & Toschi, F. 2007 Heavy particle concentration in turbulence at dissipative and inertial scales. *Phys. Rev. Lett.* **98**, 084502.

Bracco, A., Chavanis, P. H., Provenzale, A. & Spiegel, E. A. 1999 Particle aggregation in a turbulent Keplerian flow. *Physics of Fluids* **11** (8), 2280–2287.

Deepu, P, Ravichandran, S & Govindarajan, Rama 2017 Caustics-induced coalescence of small droplets near a vortex. *Physical Review Fluids* **2** (2), 024305.

Drazin, Philip G & Reid, William Hill 2004 *Hydrodynamic stability*. Cambridge university press.

Falkovich, G, Fouxon, A & Stepanov, M G 2002 Acceleration of rain initiation by cloud turbulence. *Nature* **419** (6903), 151–154.

Gatignol, R 1983 The faxén formulae for a rigid particle in an unsteady non-uniform stokes flow. *J. Mec. Theor. Appl.* **2**, 143–160.

Guasto, Jeffrey S., Rusconi, Roberto & Stocker, Roman 2012 Fluid mechanics of planktonic microorganisms. *Annual Review of Fluid Mechanics* **44**, 373–400.

Izbassarov, Daulet, Rosti, Marco E., Ardekani, M. Niazi, Sarabian, Mohammad, Hormozi, Sarah, Brandt, Luca & Tammisola, Outi 2018 Computational modeling of multiphase viscoelastic and elastoviscoplastic flows. *International Journal for Numerical Methods in Fluids* **88** (12), 521–543.

Joshi, Harshit, Chajwa, Rahul, Ramaswamy, Sriram, Menon, Narayanan & Govindarajan, Rama 2025 Dynamics and clustering of sedimenting disc lattices. *Journal of Fluid Mechanics* **1017**, A1.

Kapoor, Saumav, Jaganathan, Divya & Govindarajan, Rama 2024 Trapping and extreme clustering of finitely dense inertial particles near a rotating vortex pair. *Journal of Fluid Mechanics* **996**, A44.

Kumar, Anup & Govindarajan, Rama 2024 Mechanism of instability in non-uniform dusty channel flow. *Journal of Fluid Mechanics* **997**, A77.

Lasheras, Juan C. & Tio, Kek-Kiong 1994 Dynamics of a Small Spherical Particle in Steady Two-Dimensional Vortex Flows. *Applied Mechanics Reviews* **47** (6S), S61–S69.

Lin, CC 1945*a* On the stability of two-dimensional parallel flows. ii. stability in an inviscid fluid. *Quarterly of Applied Mathematics* **3** (3), 218–234.

Lin, CC. 1945*b* On the stability of two-dimensional parallel flows: Part i.—general theory. *Quarterly of Applied Mathematics* **3** (2), 117–142.

Lin, CC. 1946 On the stability of two-dimensional parallel flows. iii. stability in a viscous fluid. *Quarterly of Applied Mathematics* **3** (4), 277–301.

Marcu, B., Meiburg, E. & Newton, P. K. 1995 Dynamics of heavy particles in a Burgers vortex. *Physics of Fluids* **7** (2), 400–410.

Marshall, J. S. 1998 A model of heavy particle dispersion by organized vortex structures wrapped around a columnar vortex core. *Physics of Fluids* **10** (12), 3236–3238.

Marshall, J. S. 2005 Particle dispersion in a turbulent vortex core. *Physics of Fluids* **17** (2), 025104.

Maxey, M. R. & Riley, J. J. 1983 Equation of motion for a small rigid sphere in a nonuniform flow. *Physics of Fluids* **26** (4), 883–889.

Moffatt, HK, Kida, S & Ohkitani, Koji 1994 Stretched vortices–the sinews of turbulence; large-reynolds-number asymptotics. *Journal of Fluid Mechanics* **259**, 241–264.

Rajarshi, C & Govindarajan, Rama 2026 Caustics of finitely dense inertial particles. *arXiv preprint arXiv:2601.14179* .

Raju, N. & Meiburg, E. 1997 Dynamics of small, spherical particles in vortical and stagnation point flow fields. *Physics of Fluids* **9** (2), 299–314.

Ramadugu, Rashmi, Perlekar, Prasad & Govindarajan, Rama 2022 Surface tension as the destabiliser of a vortical interface. *Journal of Fluid Mechanics* **936**, A45.

Ravichandran, S & Govindarajan, Rama 2015 Caustics and clustering in the vicinity of a vortex. *Physics of Fluids* **27** (3).

Ravichandran, S. & Govindarajan, Rama 2022 Waltz of tiny droplets and the flow they live in. *Phys. Rev. Fluids* **7**, 110512.

Ravichandran, S, Perlekar, Prasad & Govindarajan, Rama 2014 Attracting fixed points for heavy particles in the vicinity of a vortex pair. *Physics of Fluids* **26** (1).

Sapsis, T. & Haller, G. 2010 Clustering criterion for inertial particles in two-dimensional time-periodic and three-dimensional steady flows. *Chaos* **20** (1), 017515.

Squires, K. D. & Eaton, J. K. 1991 Preferential concentration of particles by turbulence. *Physics of Fluids A* **3** (5), 1169–1178.

Tio, Kek-Kiong, Liñán, Amable, Lasheras, Juan C. & Gañán-Calvo, Alfonso M. 1993 On the dynamics of buoyant and heavy particles in a periodic stuart vortex flow. *Journal of Fluid Mechanics* **254**, 671–699.

Van Dyke, Milton 1964 *Perturbation Methods in Fluid Mechanics*. New York: Academic Press.

Varaksin, A. Y. & Ryzhkov, S. V. 2022 Vortex flows with particles and droplets (a review). *Symmetry* **14** (10).

Wilkinson, Michael, Mehlig, Bernhard & Bezuglyy, Vlad 2006 Caustic activation of rain showers. *Phys. Rev. Lett.* **97**, 048501.